

Lipid phase behavior studied with a quartz crystal microbalance: A technique for biophysical studies with applications in screening

Astrid Peschel,¹ Arne Langhoff,¹ Eva Uhl,² Aruna Dathathreyan,^{1,3} Susanne Haindl,^{1,2} Diethelm Johannsmann¹ and Ilya Reviakine^{2,4,a)}

¹*Institute of Physical Chemistry, Clausthal University of Technology, 38678 Clausthal-Zellerfeld, Germany*

²*Institute of Functional Interfaces (IFG), Karlsruhe Institute of Technology (KIT), Hermann-von Helmholtz-Platz 1, 76344 Eggenstein-Leopoldshafen, Germany*

³*CSIR-CLRI, Adyar, Chennai 600020, India*

⁴*Department of Bioengineering, University of Washington, Seattle, Washington 98105, USA*

(Received 23 September 2016; accepted 8 November 2016; published online 30 November 2016)

Quartz crystal microbalance (QCM) is emerging as a versatile tool for studying lipid phase behavior. The technique is attractive for fundamental biophysical studies as well applications because of its simplicity, flexibility, and ability to work with very small amounts of material crucial for biomedical studies. Further progress hinges on the understanding of the mechanism, by which a surface-acoustic technique such as QCM, senses lipid phase changes. Here, we use a custom-built instrument with improved sensitivity to investigate phase behavior in solid-supported lipid systems of different geometries (adsorbed liposomes and bilayers). We show that we can detect a model anesthetic (ethanol) through its effect on the lipid phase behavior. Further, through the analysis of the overtone dependence of the phase transition parameters, we show that hydrodynamic effects are important in the case of adsorbed liposomes, and viscoelasticity is significant in supported bilayers, while layer thickness changes make up the strongest contribution in both systems. *Published by AIP Publishing.* [<http://dx.doi.org/10.1063/1.4968215>]

INTRODUCTION

Lipid bilayers are the building blocks of cell membranes.^{1,2} Therefore, their organization and behavior continue to be intensely studied.^{3,4} Of particular interest are transitions between different lipid phases^{5,6} as they pertain to cell membrane organization and dynamics.^{4,6–8} These basic phenomena are of direct clinical relevance, for example, in the context of how anesthetics affect the conduction of the action potentials along the axon fibers and the corresponding transmembrane ion currents underlying this process.^{9,10} The connection between the action of anesthetics and lipid membrane properties was established in late 1800s through the so-called Meyer-Overton correlation between lipid solubility of the anesthetic compounds and their potency. A mechanism of anesthetic action based on their effect on the lipid phase behavior had also been proposed.^{7,8} Subsequently, the ion channel hypothesis dominated the field. The subject has recently been reviewed by Lugli *et al.*¹⁰ According to the current view, anesthetic function is not adequately described by either the lipid or the ion channel hypotheses.¹⁰ Modern theories invoke anesthetic effects on the lipid bilayer lateral pressure profile, which is thought to couple to the function of the ion channels.¹¹ Studies of anesthetic-lipid interactions *viz-a-viz* their effect on the lipid phase behavior are therefore of considerable interest to resolve the remaining controversy. Such studies can also provide a foundation for the development of biosensors for detecting lipophilic and membrane-binding substances.¹² Applications

of these approaches are diverse, including the possibility of developing closed-loop anesthesia.

Key parameters that characterize phase transitions include the transition temperature (T_M for the main transition between the gel and the fluid phases), transition enthalpy, and cooperativity. These are measured in calorimetry experiments by monitoring the heat flow to/from the lipid suspension in water as a function of temperature. At the transition, the heat flow goes through an extremum, which defines the transition temperature; the cooperativity is related to the width of the peak, while the transition enthalpy is the area under the peak. Differential scanning calorimetry (DSC), where a solvent-containing reference cell is used to define a baseline, has been used for many decades to study lipid phase behavior.^{5,13} Transition temperatures of pure lipids and their mixtures with cholesterol,^{5,14,15} as well as the effects of additives such as ethanol—a model anesthetic—have been investigated in much detail.^{16–18} DSC experiments with phosphatidyl cholines (PCs) and PC-cholesterol mixtures are so robust that they are used in undergraduate laboratory experiments;¹⁹ they can therefore be used to calibrate other methods.

Despite the versatility of DSC, there is a need for complementary label-free methods for studying lipid phase behavior. First, screening applications require miniaturization and parallelization that are not easily undertaken with DSC. Second, many biophysical methods used to study lipid systems work with non-trivial geometries such as single monolayers or bilayers, which are hardly amenable to DSC. Examples of such methods include neutron and X-ray reflectometry, techniques that are routinely used to study anesthetic action on lipid bilayers.^{20,21}

^{a)} Author to whom correspondence should be addressed. Electronic mail: reviakine@uw.edu. Tel.: +49 721 608 22991. Fax: +49 721 608 23478.

An emerging method for studying lipid-phase behavior that efficiently detects and quantifies phase transitions in lipids down to the level of a single lipid bilayer is the quartz crystal microbalance (QCM or QCM-D). The QCM is a rather simple device and is therefore well suited for sensing and routine testing. It consists of a plate of crystalline quartz vibrating in the thickness-shear mode. The resonance frequency of a bare crystal is determined by its thickness, while changes of the resonance frequency and the resonance bandwidth reveal (combinations of) surface-adsorbed mass, near-field viscoelasticity changes, and hydrodynamic effects, depending on the experimental conditions. The technique and data interpretation strategies have been recently reviewed by us.²² Keller and Kasemo were first to demonstrate that lipid assemblies with different morphologies, such as single supported lipid bilayers (SLBs) or supported vesicular layers (SVLs), elicit different responses from a QCM: SLBs hardly affect the dissipation (at the same time reducing the frequency by about 25 Hz), while SVLs *do* increase the dissipation factor appreciably.²³ Also, the frequency shift is much larger for SVLs than for SLBs. Both types of assemblies have recently been used to detect phase transitions in lipid systems.^{24–27} Considering that an SLB contains ~ 500 ng/cm² of lipid material, and an SVL ~ 1200 ng/cm², the QCM is extremely sensitive. It is also applicable to biological samples that are typically available only in minute amounts, since volumes of less than 100 μ l can be used with modern fluid cells. Even less is needed to prepare an SLB or an SVL on the resonator surface that can then be studied in the presence of excess buffer.

Capitalizing on these potential benefits of the QCM-based approach, we use this method to detect a model anesthetic through its effect on the phase transition parameters in lipid bilayers (SLBs) and surface-adsorbed vesicles (SVLs), to show that adsorbed vesicle-to-bilayer transformation is not a pre-requisite for these measurements. Aside from the fundamental interest, we explore the extent to which this methodology might be useful for routine investigations, such as screening. We also examine efficient ways to aggregate data, the stability of the lipid assemblies under repeated cycling, and mechanism by which QCM senses the transition in assemblies of different geometries (SVLs and SLBs).

MATERIALS AND METHODS

Lipids and liposome preparation

1,2-dimyristoyl-sn-glycero-3-phosphocholine (DMPC) was purchased from Avanti Polar Lipids (Alabaster, AL, USA) as a powder and stored at -20 °C until used. The liposome preparation protocols we used have been described in previous publications.^{28,29} In short, the lipid powder was dissolved in chloroform. Chloroform was evaporated with a stream of nitrogen to form a thin film on the walls of a round-bottom test tube. The lipid film was dried under vacuum of 80 mbar provided by a Buchi (Flawil, Switzerland) dry vacuum pump for at least 1 hr, at which point the lipid was resuspended in a buffer containing 10 mM HEPES, 150 mM NaCl, and 2 mM CaCl₂, pH 7.4, by vortexing at a temperature above the transition temperature of the lipid or lipid mixture, to form multilamellar vesicles (MLVs). The buffer was filtered through 200 nm pore diameter

syringe filters (FP 30/0.2 CA-S Whatman Puradisc Cellulose Acetate, purchased from VWR International GmbH, Bruchsal, Germany) immediately before use. Unilamellar liposomes used in QCM experiments were prepared from the MLVs by extrusion through 50 nm pore diameter filters using a hand-held LipoFast extruder (Avestin, Ottawa, Canada).³⁰ Extrusion was performed above the main transition temperature of the relevant lipid or lipid mixture. The water used in this study was purified with an Arium® Pro VF Ultrapure water system from Sartorius (Göttingen, Germany).

Quartz crystal microbalance (QCM) experiments

Experiments were performed with a home-built, impedance-based QCM consisting of an impedance (network) analyzer for determining resonance frequencies and bandwidths of a quartz crystal,³¹ and a fluid cell, also home-built, where the crystals were mounted, to allow liposome adsorption, fluid exchange, and temperature control. The network analyzer was purchased from Ivan Makarov (makarov.ca). The resonance frequencies and bandwidths were collected on overtones, n , between 3 and 11, corresponding to frequencies between 15 and 55 MHz.

Following the prevalent practice in the field, we quantify dissipative processes using the dissipation factor (“dissipation,” for short), D , defined as the ratio of full bandwidth of the resonance to the resonance frequency (the inverse Q-factor). As usual, values for the frequency shift are scaled by the overtone order; that is, we discuss $\Delta f/n$ rather than Δf . The reason is that $\Delta f/n$ is the same on all overtones if the frequency shift is caused by gravimetric effects. Dissipation changes are not scaled by the overtone order because such a scaling by n is implicitly contained in the definition of D (D is the ratio of bandwidth to frequency, where the latter scales as n).

Silica-coated AT-cut quartz crystals with a diameter of 14 mm and a fundamental frequency of 5 MHz (Biolin Scientific, Gothenburg, Sweden) were used for the study of SLBs. Gold-coated resonators purchased from SuZhou SJ Biomaterials, Suzhou, China, were used in the experiments on the supported vesicle layers. Immediately prior to each experiment, crystals were cleaned in 2% SDS solution that was freshly filtered through 0.2 μ m pore diameter filters, rinsed with water, and treated in a UV-Ozone (Bioforce Nanosciences, Ames, AL, USA) cleaner for 30 min. The UV-Ozone cleaner was pre-heated for 30 min immediately before use.

Our work builds heavily on the temperature-derivatives of f and D . Low noise is critical. The central step towards noise reduction was to connect the crystal to the network analyzer in transmission rather than in reflection, which is the more common procedure. When immersed in liquids, the resonator’s electrical resistance, R_1 , is much higher than 50 Ω , which brings the electrical signal as detected in reflection close to unity. The analysis of the resonance relies on a small difference between two large numbers. Detection in transmission is more efficient in this regard because it occurs against a background of zero. Because R_1 is large, the transmitted signal is small. Discerning a small signal from a vanishing background is easier than discerning a large signal from a significant background. The details of the argument involve a set of algebraic transformations, which lead from the raw

signal at the detector to the impedance of the device under test. These transformations involve calibration. They are outside the scope here. Detection in transmission entails a complication insofar, as additional measures must be taken to ensure that the front electrode is grounded. (When the measurement is done in reflection, the grounding of the front electrode occurs through the ground of the analyzer.) If the front electrode is not grounded, liquid conductance in conjunction with effects of piezoelectric stiffening can produce artifacts.^{32,33} Grounding of the front electrode was achieved by inserting a transformer (ADT 1-1, Minicircuits) between the resonator and the driving electronics as shown in Figure 1. One leg of the transformer connects both to the front electrode and to ground, which solves the problem.

The noise level achieved in this configuration, $\delta f_{pp}/n$, was ~ 30 mHz/Hz^{1/2} for the frequency and 12×10^{-9} /Hz^{1/2} for the dissipation factor on the low overtones (15 and 25 MHz). It increases by about a factor of 2 on the higher overtones. (We quote the noise in the overtone-normalized frequency, hence the division by n .) The noise was defined as

$$\delta f_{pp} = \sqrt{\frac{1}{2} \langle (f_{i-1} - 2f_i + f_{i+1})^2 \rangle} t_{pp}. \quad (1)$$

f_i is the i th frequency reading and t_{pp} is the time per frequency sweep. Angular brackets denote averaging. An analogous equation was used for the dissipation factor. This definition of point-to-point fluctuations is conceptually related to the Hadamard variance, defined as $\delta f_{Had}^2 = \langle (f_{i-1} - 2f_i + f_{i+1})^2 \rangle / 6$. Because the definition builds on three successive frequency readings, rather than two, it eliminates the influence of a frequency drift on the calculated noise. The time per sweep, t_{pp} , is included into the definition of the noise because slow frequency sweeps will improve the signal-to-noise ratio—at the expense of speed. (Averaging over successive data points achieves the same.) In order to account for the (perfectly common) trade-off between speed and precision, we divide the noise-power (the noise-squared) by the bandwidth of data acquisition—which in this case amounts to multiplication by t_{pp} . Noise figures are then quoted with the respective numbers (Hz and 10^{-6} for $\Delta f/n$ and ΔD , respectively) divided by Hz^{1/2}. A value of 30 mHz/Hz^{1/2} then implies that the point-to-point fluctuations are 30 mHz if the frequency sweeps last for 1 s. Note, that δ in Eq. (1) represents rms noise, while Δ in $\Delta f/n$ and ΔD represents finite difference, referred to in the literature as a shift in the frequency or the dissipation.

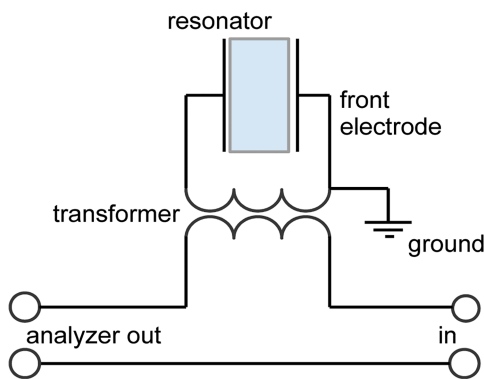


FIG. 1. Scheme of wiring a resonator in transmission.

Temperature was controlled with a programmable water-based thermostat. The thermocouple was integrated into the base of the cell. The digital output of the thermometer had a resolution of 0.1 °C, which is insufficient for the analysis based on temperature derivatives. To allow for meaningful temperature derivatives, a time-temperature-relation with a precision better than 0.1 °C was created by fitting a third-order polynomial to temperature-vs-time curves. The nominal temperature supplied by the thermometer was then replaced by the interpolated values resulting from this fit. Using this time-temperature relation, the time dependence of frequency and dissipation was converted into the temperature dependence, where phase transitions appear as steps. Differentiation with respect to temperature turns steps into peaks. Importantly, the scatter in the temperature-derivatives of frequency and dissipation obtained through the interpolation of the time-temperature data is dominated by the scatter in $\Delta f/n$ and ΔD , with no contribution from scatter in the temperature. An example of a peak in the temperature derivative is shown in Figure 2. In order to allow for comparison between experiments, the plots of the derivatives vs. temperature were reduced to three parameters: the center of each such peak (T_{cen} , in units of °C), the width of the peak (T_{wid} , also in units of °C), and the integral over the peak (I , in units of Hz for $\Delta f/n$ and in units of 10^{-6} for D). A baseline was defined by fitting a straight line to the data in a certain range to the right and to the left of the features of interest before the computations. The range of data to be used for the baseline was selected by hand. The data reduction procedure based on the derivatives emphasizes the analogy with DSC and is compatible with the existing literature on the phase transitions of lipids detected with a QCM.

More quantitatively, T_{cen} , T_{wid} , and I were computed using the following set of equations:

$$I = \sum_{i=\min}^{\max} (g'(T_i) - g'_{BL}(T_i)) \Delta T_i = \sum_{i=\min}^{\max} w_i \Delta T_i,$$

$$T_{cen} = \frac{\sum_{i=\min}^{\max} w_i T_i \Delta T_i}{\sum_{i=\min}^{\max} w_i \Delta T_i}, \quad (2)$$

$$T_{wid}^2 = \frac{\sum_{i=\min}^{\max} w_i (T_i - T_{cen})^2 \Delta T_i}{\sum_{i=\min}^{\max} w_i \Delta T_i}.$$

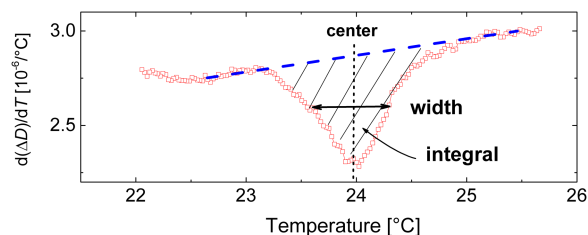


FIG. 2. Schematic of the data reduction process. This is an example of the derivative of the dissipation shift with respect to temperature. The transition parameters (center, width, and integral, the latter cross-hatched area under the peak) are indicated in the figure. The baseline is shown in blue. (cf. with Figure 1 in Ref. 13, where similar definitions for DSC are presented.)

g here is either the overtone-normalized frequency shift ($\Delta f/n$) or the shift in dissipation (ΔD). The prime denotes differentiation with respect to temperature. The difference between the derivatives and the baseline (see Figure 2) takes the role of a statistical weight, w_i . As usual, the integral, the center, and the width are closely related to the 0th, the 1st and the 2nd moment of the distribution of w_i .

RESULTS

The model systems: Supported lipid bilayers (SLBs) and vesicle layers (SVLs)

The first step in our study was to prepare the two model systems: the SLBs on silica (Figure 3) and the SVLs on gold (Figure 4). To this end, we followed SLB formation from DMPC liposomes on the silica surface as a function of temperature in a series of liposome adsorption experiments. Each experiment proceeded as follows: a freshly cleaned QCM crystal was equilibrated with buffer to achieve a stable baseline. An aliquot of the liposome suspension in buffer at a lipid concentration of 0.2 mg/ml, pre-equilibrated at the desired temperature, was added to the fluid cell, and the QCM response was followed as a function of time under stagnant conditions. The results are shown in Figure 3.

At temperatures below T_M (which is at 24 °C for DMPC⁵), the QCM response was typical of intact liposome adsorption:²³ the asymptotic dissipation shifts, ΔD , were large, and

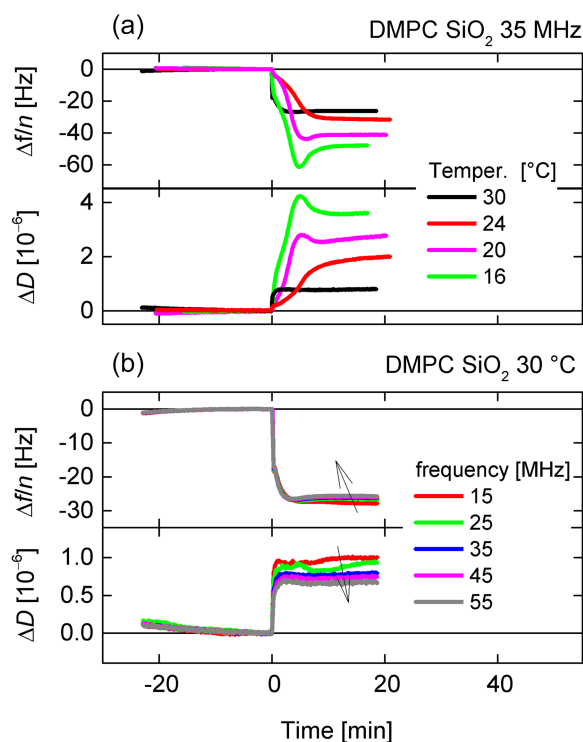


FIG. 3. Supported lipid bilayer formation from DMPC liposomes on silica. (a) 50 nm DMPC liposomes were allowed to adsorb on SiO₂-coated QCM crystals at different temperatures (indicated on the plot). The results for the 7th overtone (35 MHz) are shown. (b) Results of the adsorption experiment performed at 30 °C. Data on different overtones are shown. Arrows indicate increasing overtone order. Δf and ΔD refer to the differences in frequency and dissipation shifts relative to the values observed in buffer prior to the introduction of liposomes. Liposomes were introduced at time 0. Frequency shifts are scaled by the overtone order n .

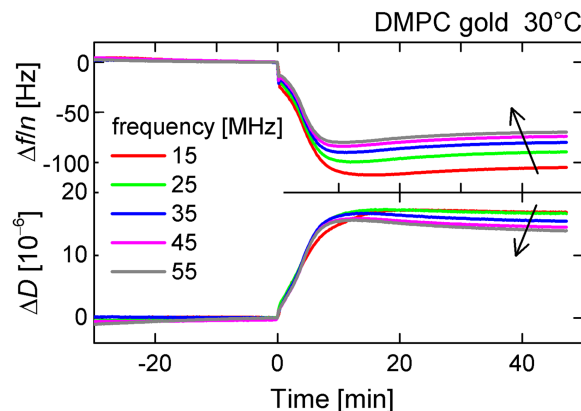


FIG. 4. Supported vesicular layer formation on gold. 50 nm DMPC liposomes were allowed to adsorb on an Au-coated QCM crystal at 30 °C. Data on different overtones are shown. Arrows indicate increasing overtone order.

the asymptotic frequency shifts, $-\Delta f/n$, were significantly larger than 25 Hz expected of an SLB.²³ Asymptotic frequency and dissipation shifts decreased as the temperature,

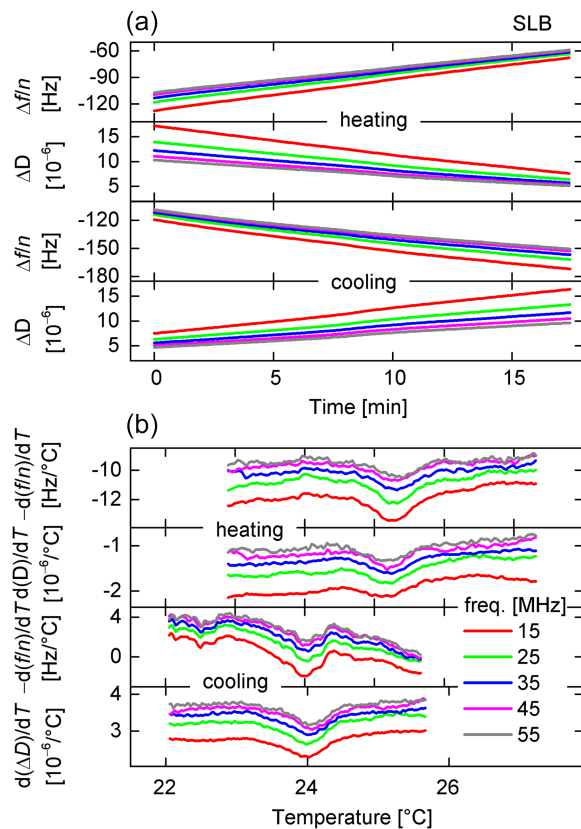


FIG. 5. Detecting lipid phase transitions in an SLB. (a) A sequence of the heating/cooling cycles performed on the sample, the generation of which is documented in Figure 2(b). Data from overtones 3 (red) to 11 (gray) are shown. As is often the case with quartz resonators, the fundamental behaves differently from the other overtones and is therefore not shown. The suspected reasons are the flexural contributions to the vibration fields and electric fringe fields producing artifacts because piezoelectric stiffening. (b) These plots show the derivatives of the frequency and dissipation shifts ($d(\Delta f/n)/dT$ and $d(\Delta D)/dT$) with respect to temperature obtained on heating and cooling cycles. To obtain the derivatives, the time axes of the plots shown in (a) were converted into temperature by fitting the time-temperature data with a third-order polynomial as described in the Materials and Methods Section. Peaks in the derivatives are visible both on heating and cooling cycles. The scan rate was 0.2 °C/min.

at which the adsorption experiments were performed, approached T_M , tending to ~ 27 Hz and $\sim 0.4 \times 10^{-6}$, respectively, at 30°C (Figure 3). As we discuss below, we interpret this as evidence of SLB formation.

This type of temperature-dependent behavior (SVL formation at $T < T_M$ and SLB formation at $T > T_M$) has been described previously by other authors. Most recently, Wacklin *et al.* combined QCM with neutron reflectometry and atomic force microscopy to examine the behavior of dipalmitoyl phosphatidylcholine (DPPC) liposomes adsorbing on silica above and below its main transition temperature.³⁴ Their QCM traces are similar to the ones we show in Figure 3(a) and were correlated with the AFM images to show that an SVL formed below the main transition temperature of DPPC, while an SLB—above. The intermediate behavior reported by Wacklin *et al.* is also similar to what we present here (Figure 3(a)). Earlier, Seantier *et al.* presented similar observations for DMPC.³⁵

The asymptotic frequency and dissipation shifts, which we finally observed with the SLBs (Figure 3), are somewhat higher than the classical literature values associated with the bilayer formation.²³ Also, the asymptotic frequency shifts were not the same on all overtones (Figure 3(b)). This typically indicates finite compliance. One may apply the acoustic multilayer formalism^{32,36,37} to the data and derive values for an apparent viscoelastic compliance $J = J' - iJ''$ (or, equivalently, for an apparent modulus $G = G' + iG''$, G being the inverse of J). Indeed, doing this kind of viscoelastic analysis on different samples, we found a considerable variability in

values derived for J . We never found J to be compatible with zero, though. Most likely, the slightly higher ΔD and $\Delta f/n$ values as well as the dependence of $-\Delta f/n$ on n originate from a few vesicles that remain associated with our SLBs due to trace surface contamination. This, however, does not affect our subsequent results.

DMPC liposomes adsorbing on gold at a temperature above T_M remained intact (Figure 4). This is consistent with previously published observations of phosphatidylcholine liposomes adsorbing on gold at a $T > T_M$.²³

In summary, we formed SLBs on SiO_2 and SVLs on gold by adsorbing DMPC liposomes at 30°C , which is above the

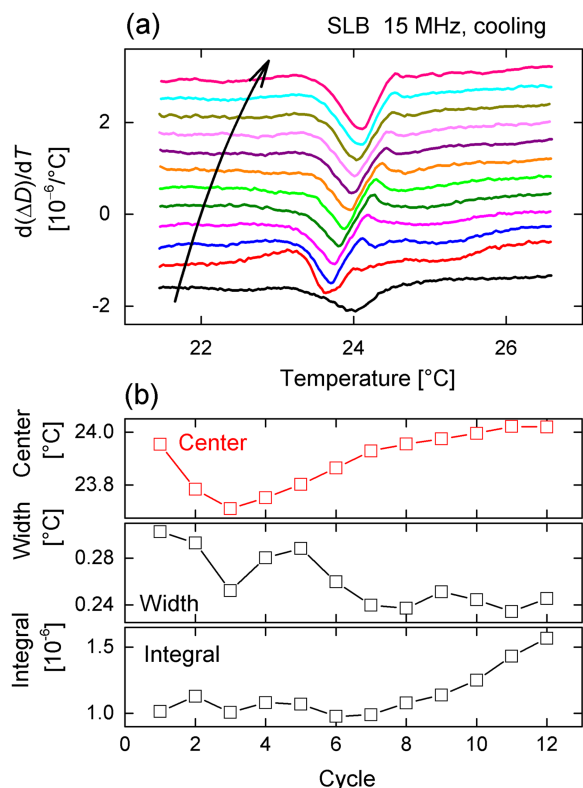


FIG. 6. SLB annealing. (a) The peaks in the derivatives become better defined upon repeated heating/cooling cycling. (b) Evolution of the transition parameters—peak center, width, and integral—with repeated cycling. Dissipation data obtained on the 3rd overtone (15 MHz) upon cooling are shown. The scan rate was $0.2^\circ\text{C}/\text{min}$.

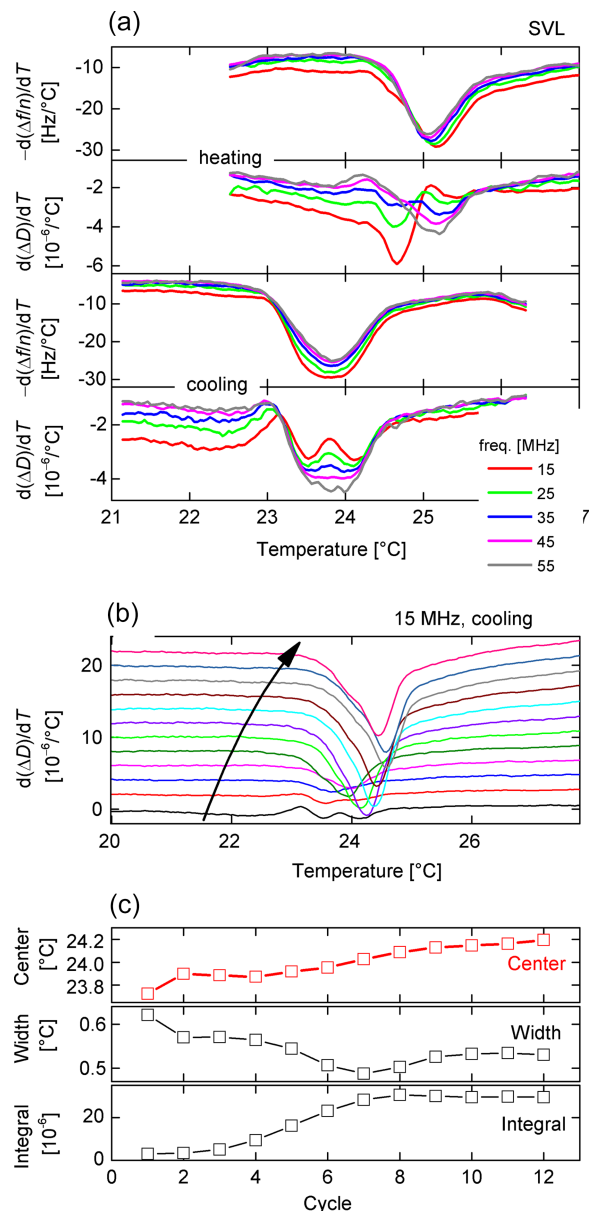


FIG. 7. Detecting lipid phase transitions in an SVL. (a) These are the temperature derivatives obtained on the heating/cooling cycles applied to an SVL, such as the one shown in Figure 4. The procedure was the same as that followed for the SLBs. (b) The evolution of the transition peak upon repeated cycling (annealing). Frequency data obtained on cooling on the 3rd overtone (15 MHz) are shown. (c) The evolution of the peak maximum, width, and integral with repeated cycling. The corresponding data derived from $\Delta f/n$ (rather than ΔD) are presented in Figure S1 in the supplementary material. The scan rate was $0.2^\circ\text{C}/\text{min}$.

T_M of DMPC. We conducted further studies with these two model systems as described below. Unless stated otherwise, the samples were rinsed with the buffer before subsequent experiments to avoid the contribution from the liposomes in solution. Rinsing is critical. As will be reported in a separate publication, lipid multilayers form if the temperature cycles are carried out in the presence of a dispersion of liposomes.

Phase transitions in SLBs and SVLs detected with a QCM

Temperature sweeps on SLBs are shown in Figure 5(a). There is a smooth dependence of the $\Delta f/n$ and ΔD on temperature. As previously shown by several other authors,^{24–26} this dependence is unrelated to the state of the lipids: it is mostly due to the changes in the viscosity of the liquid as a function of temperature: lowering the temperature increases the viscosity and the damping of the resonance and decreases the frequency, as shown by Kanazawa and Gordon.^{38,39} For Δf , there is an additional contribution of the intrinsic temperature-frequency coupling of the resonator. The temperature-frequency coupling is small for AT-cut quartz, but it can only be made to vanish on one single overtone (which is the fundamental for the crystals employed here). For all other overtones, the temperature-frequency coupling coefficient is of the order of a few ppm/°C.

As a consequence of these various effects of temperature unrelated to the lipids' behavior, the parameters of the transition cannot be read out from the QCM measurements directly. Several approaches exist to extract them. Ohlsson *et al.*²⁴ and later Losada-Pérez *et al.*²⁶ performed a reference measurement with the bare crystal, the results of which were subtracted from the (crystal + lipid) measurement. This allowed the phase transitions to be examined using Δf and ΔD . Wargenau and Tufenkji²⁵ took the first derivative of the frequency shift with respect to temperature, while Hasan and

Mechler⁴⁰ worked with the dissipation derivative. We favor the derivative approach as it better deals with instrumental drifts and does not require the additional (reference) measurements. Also, this representation appeals to intuition because analogous plots are known from DSC. The derivatives of $\Delta f/n$ and ΔD with respect to temperature are shown in Figure 5(b). There are clearly visible peaks in both derivatives close to the expected T_M of DMPC (24 °C). It is noteworthy that the transition is more apparent in the dissipation derivative than in the frequency derivative. The peaks are visible on both the heating and the cooling cycles, as expected. Hysteresis (1.4–1.7 °C) is apparent from comparing the heating and the cooling cycles and is similar to that previously reported by others at the scan rate we used in our experiments (0.2 °C/min).^{24–26,40}

We then examined the behavior of the transition in an SLB upon repeated temperature cycling. The derivative of the dissipation with respect to temperature, obtained upon cooling, is shown in Figure 6(a). The evolution of the classical transition parameters—temperature at the peak, peak width, and integral—is summarized in Figure 6(b). The peak becomes better defined with repeated cycling; the center of the peak shifts to higher temperatures, the peak becomes narrower, and the integral grows. The integral refers to the difference in the frequency (dissipation) between the low-temperature and the high-temperature states. The sign implies that the magnitude of the frequency (dissipation) shifts increases upon cooling.

The transition could also be detected in an SVL (Figure 7). The temperature derivatives observed upon heating and cooling are shown in Figure 7(a). Here, the peaks in the frequency derivative are more robust. The peaks in both derivatives are more pronounced than in the case of an SLB (Figure 5). It is easier to detect the transition in an SVL. The peaks are also broader. The annealing behavior that is observed upon temperature cycling in an SVL (Figures 7(b) and 7(c)) is similar to that observed on an SLB (Figure 6). Note, however,

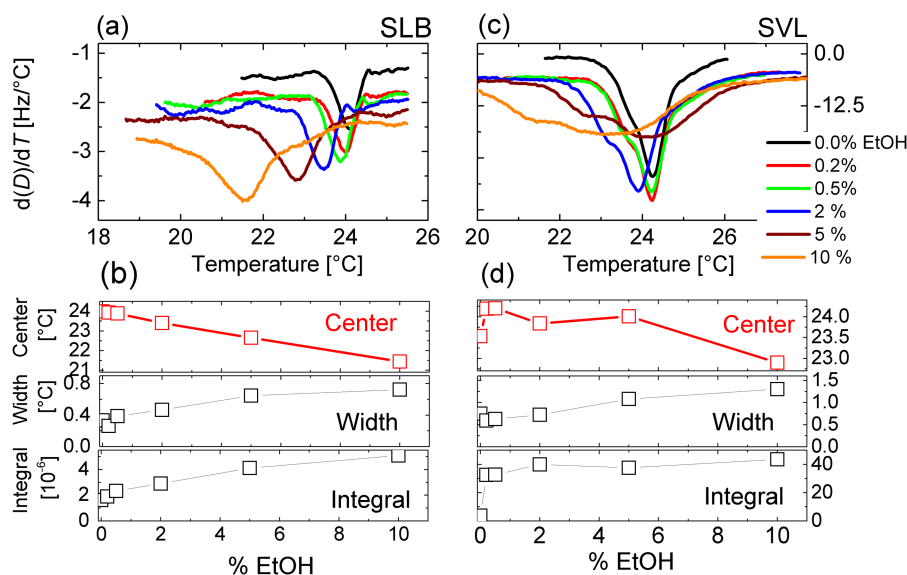


FIG. 8. Effect of ethanol on the lipid phase transition can be detected by QCM. (a) and (b) The evolution of the dissipation derivative as a function of the volume fraction of ethanol in the buffer, observed with an SLB. (c) and (d) same, but with an SVL instead of an SLB. To obtain these data, the buffer above the SLB or an SVL was exchanged with the buffer containing the specified amount of ethanol, and the temperature was cycled back and forth twice. The results of the cooling cycles, on the 3rd overtone (15 MHz) are shown. Note the different scales on the Y-axes of the panels (a) and (c), as well as the plots of the integrals in the panels (b) and (d). In the case of the SVL, the frequency derivative data are presented in Figure S2 in the [supplementary material](#).

TABLE I. Summary of transition parameters. Transition center, width, and integral, as defined in Fig. 2, obtained from the dissipation (ΔD) and frequency ($\Delta f/n$) temperature derivatives upon cooling and heating for the various model systems. *: cycles 1 + 2; **: cycles 9 - 11; ***: cycles 10 - 12.

	cooling						heating							
	ΔD			$\Delta f/n$			ΔD			$\Delta f/n$				
	Center (°C)	Width (°C)	Integrals (10 ⁻⁶)	Center (°C)	Width (°C)	Integrals (Hz)	Center (°C)	Width (°C)	Integrals (10 ⁻⁶)	Hysteresis (°C)	Center (°C)	Width (°C)	Integrals (Hz)	Hysteresis (°C)
15 MHz														
DMPC SLB*** Ethanol	24.01 ± 0.02	0.44 ± 0.03	0.57 ± 0.06				25.80 ± 0.01	0.37 ± 0.04	0.51 ± 0.04	1.79				
DMPC SLB + 0.5% EtOH*	23.87 ± 0.05	0.33 ± 0.02	0.95 ± 0.02				25.77 ± 0.04	0.43 ± 0.02	0.94 ± 0.02	1.90				
DMPC SLB + 2.0% EtOH*	23.45 ± 0.07	0.44 ± 0.04	1.14 ± 0.03				25.43 ± 0.17	0.50 ± 0.06	1.10 ± 0.10	1.98				
DMPC SLB + 5.0% EtOH*	22.74 ± 0.20	1.04 ± 0.05	2.32 ± 0.11				24.72 ± 0.04	1.25 ± 0.04	2.31 ± 0.13	1.98				
DMPC SLB + 10.0% EtOH*	21.51 ± 0.05	0.81 ± 0.01	2.36 ± 0.01				23.68 ± 0.10	1.14 ± 0.12	2.40 ± 0.38	2.17				
DMPC SVL***	24.17 ± 0.02	0.53 ± 0.01	11.82 ± 0.04	24.34 ± 0.04	0.50 ± 0.01	30.04 ± 0.34	25.52 ± 0.04	0.59 ± 0.02	13.17 ± 0.16	1.38	25.62 ± 0.05	0.61 ± 0.01	36.31 ± 0.37	1.31
DMPC SVL***	24.77 ± 0.01	0.63 ± 0.03	2.59 ± 0.02	24.65 ± 0.04	0.58 ± 0.01	31.11 ± 0.29	26.28 ± 0.07	0.59 ± 0.02	2.43 ± 0.14	1.51	26.23 ± 0.08	0.56 ± 0.01	24.09 ± 0.56	1.58
DMPC SVL** Ethanol	24.23 ± 0.04	0.38 ± 0.01	3.66 ± 0.24	24.29 ± 0.04	0.35 ± 0.01	40.27 ± 0.21	25.74 ± 0.05	0.32 ± 0.02	4.92 ± 0.26	1.51	25.74 ± 0.04	0.32 ± 0.01	33.09 ± 0.47	1.45
DMPC SVL + 0.5% EtOH*	24.18 ± 0.03	0.57 ± 0.01	12.16 ± 0.17	24.38 ± 0.04	0.54 ± 0.01	35.00 ± 0.99	25.57 ± 0.05	0.67 ± 0.02	14.88 ± 0.70	1.39	25.67 ± 0.08	0.67 ± 0.03	44.17 ± 2.90	1.29
DMPC SVL + 2.0% EtOH*	23.86 ± 0.04	0.74 ± 0.02	15.85 ± 0.21	24.09 ± 0.05	0.70 ± 0.01	48.79 ± 1.69	25.28 ± 0.14	0.76 ± 0.04	16.62 ± 0.22	1.42	25.46 ± 0.12	0.75 ± 0.03	51.97 ± 0.64	1.37
DMPC SVL + 5.0% EtOH*	23.94 ± 0.10	1.08 ± 0.02	14.84 ± 0.03	24.23 ± 0.15	0.98 ± 0.01	54.42 ± 1.51	25.37 ± 0.02	1.17 ± 0.03	16.12 ± 0.17	1.43	25.61 ± 0.01	1.02 ± 0.01	52.71 ± 0.56	1.38
DMPC SVL + 10.0% EtOH*	22.75 ± 0.13	1.28 ± 0.04	16.40 ± 0.01	22.95 ± 0.16	1.14 ± 0.04	61.08 ± 0.48	24.36 ± 0.01	1.26 ± 0.04	13.59 ± 1.32	1.61	24.47 ± 0.03	1.14 ± 0.03	49.29 ± 3.94	1.52

that the scale in Figure 7 is much expanded compared to Figure 6. While the frequency derivative appears to be better suited for detecting the transition in the case of SVLs, we continue to present the dissipation derivative for the SVLs for the sake of easy comparison with the SLBs. The corresponding plots of $d(\Delta f/n)/dT$ are presented in Figure S1 in the [supplementary material](#).

The effect of a model anesthetic on the lipid phase transition detected by QCM

The central result of our study is the ability of QCM to detect the effect of a model anesthetic, ethanol, on the lipid phase transition, as shown in Figure 8. The data for the SLBs are presented in Figures 8(a) and 8(b), and the data for the SVLs—in Figures 8(c) and 8(d) (the frequency derivative data are presented in Figure S2 in the [supplementary material](#)). Exposing both assemblies to progressively larger amounts of ethanol leads to a decrease in the peak center. This effect has been previously reported in DSC studies for the ethanol concentrations used here.^{16–18} It can also be seen in Figure 8 that ethanol broadens the transition and that the integral increases with the ethanol content. Similar results were obtained with SLBs and SVLs (cf. Figures 8(a)–8(d)), although the results with the SLBs are more robust (the dependencies on the ethanol concentration are smooth).

In Table I, we collect the data for the center of the peak upon cooling and heating, peak width, the integral, and hysteresis, observed in DMPC SLBs and SVLs at 15 MHz in the absence and in the presence of ethanol. It is evident, that the phase transition behavior we observe is quite reproducible.

DISCUSSION

The main point of our study was to examine the ability of the QCM to detect the effect of the amphiphilic additives on the lipid phase transitions in order to model the detection of the anesthetics. The results presented in Figure 8 show that the QCM is sensitive to the effect of ethanol on the main transition of the lipids in both solid-supported systems, SLBs and SVLs. Of particular importance is the observed decrease in the peak center (Table I) as a function of increasing ethanol content. This observation is noteworthy, because in the range of concentrations used in our study (<10% for DMPC), ethanol decreases T_M .^{16–18} This occurs because of its preferential partitioning into the lipid fluid phase. To the best of our knowledge, this is the first such study, although other authors have examined the effect of cholesterol²⁷ and ionic liquids⁴¹ on the lipid phase transitions by QCM. Based on this result, we consider fruitful further exploration by QCM of lipid phase behavior for biophysical studies, as well as for the detection of anesthetics, or other lipophilic compounds, in real or simulated bodily fluids (blood and plasma).

Several of our other observations merit detailed consideration. First we discuss the mechanism, by which QCM senses the transition. Both SVLs and SLBs are thicker and stiffer below T_M than above (Figure 9). The difference in the lipid bilayer thickness—40.1 Å below T_M and 35.3 Å above—is caused by the underlying difference in the area per molecule (APM) of the lipid: for DMPC, it is 47 Å² below T_M and

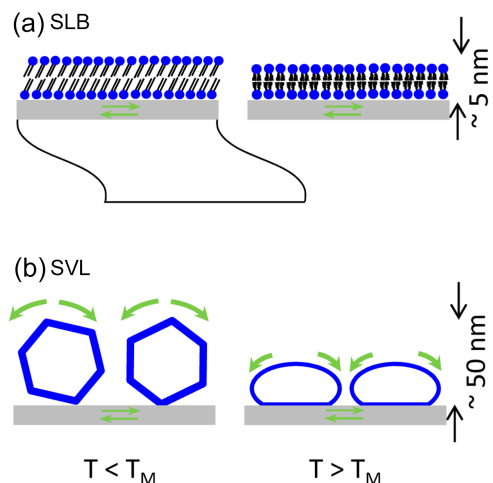


FIG. 9. Schematic illustration of the changes that occur in SLBs (top) and SVLs (bottom) across the main transition. Above T_M , the lipids are in the so-called fluid (L_α) phase. As the temperature is reduced to below T_M , the lipids find themselves in the so-called gel phase (P_β) where the area per molecule is smaller and the bilayer is correspondingly thicker. Since the gel phase is also stiffer, adsorbed liposomes take on a characteristic faceted appearance.⁴⁷ The softness of the fluid phase means that liposomes adsorbing above T_M deform and assume a characteristic dome shape.^{47,58,59} In a QCM experiment, the crystal schematically illustrated in the top left subfigure is oscillating in thickness-shear mode (straight green arrows). Therefore, the surface-supported structures are subjected to a shear field. SLBs dissipate very little, while the dissipation in the SVLs is considerable. We have previously described in detail the rocking motion and other hydrodynamic effects in SVLs (curved green arrows) that contribute to the dissipation.^{29,48,60}

60 Å² above.^{42–44} This effect is schematically illustrated in Figure 9(a). In turn, the changes in the molecular packing across the transition lead to the changes in the bilayer elastic properties: the compressibility and the bending moduli of DMPC change from ~ 0.5 N/m and 10×10^{-19} J below T_M to 0.15 N/m and $\sim 1 \times 10^{-19}$ J above T_M , respectively.^{42,44–46} This has a considerable effect on the SVL geometry, as indicated in Figure 9(b). Based on our previous results showing that liposomes adsorbing below T_M exhibited a faceted aspect and formed thicker layers, than liposomes adsorbed above T_M , which exhibited dome-shaped aspect,⁴⁷ we would expect an increase in the SVL thickness upon cooling. This is confirmed by the observation of an increase in the negative frequency shift, $-\Delta f/n$, upon cooling in DPPC SVLs by Losada-Pérez *et al.*,²⁶ and by our own observations of the peak in the frequency-temperature derivative, which indicate an increase in the magnitude of the frequency shift upon cooling and a decrease upon heating. Furthermore, based on our previous work on the dissipation processes in SVLs,⁴⁸ we conclude that there will be additional dissipation channels in SVLs below T_M connected with the hydrodynamic effects arising from their geometry. What we are concerned with here is the relative contribution of these effects (thickness, stiffness, and the dissipation channels of hydrodynamic origin) to the observed changes in the QCM signals.

Changes in the film thickness contribute to the changes in the frequency shifts in an overtone-independent manner according to the Sauerbrey relationship.⁴⁹ Changes in the viscoelastic properties contribute to the changes in the frequency shift in an overtone-dependent manner and serve to attenuate the contribution of the thickness,^{32,36,37} but their effect is

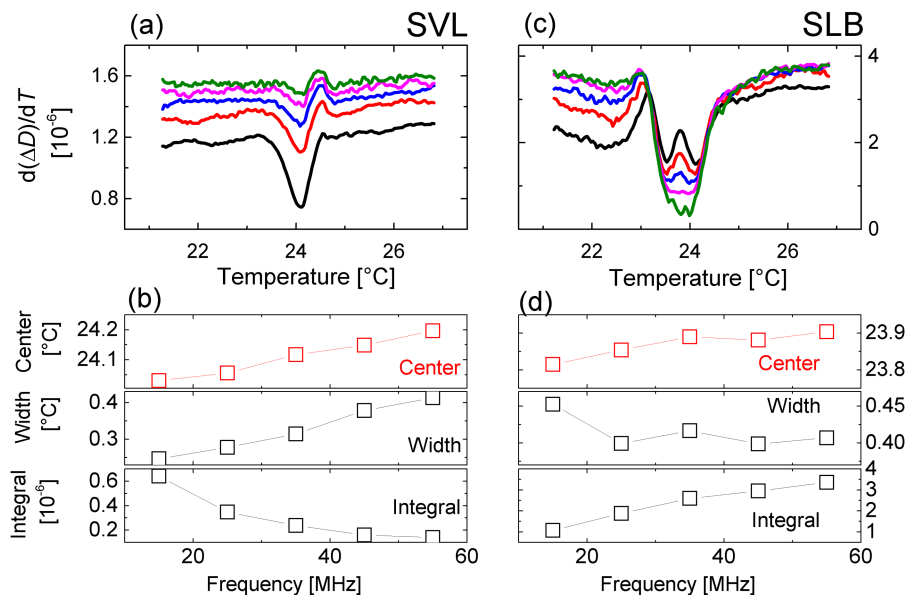


FIG. 10. Overtone dependence of the transition parameters measured with the SLBs (a) and SVLs (b). For the 5 MHz crystal used in this study, the 3rd overtone corresponds to the frequency of 15 MHz, 5th to 25 MHz, and so on, until the 11th overtone at 55 MHz. The data for the temperature derivative of the dissipation are shown. The corresponding frequency data can be found in the [supplementary material](#) Figures S3 and S4 for the SVLs and the SLBs, respectively.

smaller for the stiffer layers and greater for the softer layers. In other words, both the stiffness and the thickness changes in the lipid layer properties across the transition contribute to the increase in the frequency shift upon cooling. This effect is relevant in SLBs as well as SVLs.

In the case of the dissipation changes, the stiffness and the thickness contributions oppose each other, because stiffer layers dissipate less. In the SLBs, this leads to an overtone dependence of the transition peak: it can be seen in Figure 10 that the peak diminishes with the increasing overtone order (increasing frequency). This occurs because the stiffness contribution increases relative to the thickness contribution due to the decreasing penetration depth at higher frequencies. We therefore conclude that in the case of the SLBs, the dominant mechanism, by which QCM detects the transition, is related to the change in thickness, but that we are also able to detect the contribution of the changes in the viscoelastic properties of the SLBs. Thickness changes have been used by others to explain QCM results obtained with the SLBs undergoing a phase transition,²⁵ while viscoelastic effects until now have only been reported for suspended bilayers.⁴⁰

The observation of the viscoelastic effects in SLBs has a wider significance. SLBs have been associated with negligible levels of dissipation since their original observation by QCM by Keller and Kasemo.²³ What remained unclear is whether they were too thin for their viscoelastic properties to be detected by QCM, or too stiff, exhibiting Sauerbrey behavior. The limited detection sensitivity prevented further investigation. In light of our findings, it would appear that the former is true. Although this conclusion is consistent with some of the previously published statements,^{24,40} we must offer a cautionary note: as we remarked in the Results section, our bilayers are associated with dissipation values that are larger than usual.

In SVLs, the attenuation of the thickness contribution to the dissipation changes by that of the changes in the layer

stiffness is counteracted by the additional (hydrodynamic) dissipation channels that arise below T_M . This complicates the behavior of the dissipation derivative: Indeed, when comparing the behavior of the frequency and dissipation derivatives obtained with the SLBs (Figure 5(b)) and with the SVLs (Figure 7(a)), it is apparent that in the latter case (SVLs), the frequency derivative displays more robust features at the transition than the dissipation derivative, while in the former case (SLBs), the opposite is true. For the same reason, the values of the dissipation integral are significantly larger in the case of the SVLs than SLBs (a factor of ~ 10 , cf. Figure 7(c) and Figure 6(b)), even though the amount of lipid material in the two structures is expected to differ only by a factor of ~ 2.5 . In other words, in the case of the SVLs, layer thickness changes and hydrodynamic effects appear to dominate the mechanism by which QCM detects the transition. This conclusion is supported by the fact that the transition parameters are nearly overtone-independent in the case of the SVLs (Figure 10 and Figure S3 in the [supplementary material](#)).

The second striking observation is the behavior of the width of the transition peak under the different experimental conditions used in our study. In calorimetry experiments, transition width is related to the cooperativity (the number of lipid molecules undergoing the transition simultaneously); the more cooperative the transition, the narrower the peak. In free-standing (as opposed to solid-supported) systems composed of pure lipids, the main transition is highly cooperative at low scanning rates.⁵⁰ Both the presence of the solid support and curvature widen the transition.⁵⁰ Our values of the peak width are surprisingly close to those expected from calorimetry, and they are observed to decrease with the number of annealing cycles (Figure 6(b), Figure 7(c)), but they increase with the ethanol content (Figure 8). The fact that the peak width changes in the opposite directions upon annealing and with ethanol content, and the fact that the transition is broader in SVLs than in SLBs, as expected, rule out instrumental artifacts. However,

the observation that peak width increases with ethanol content indicates contributions unrelated to the changes in transition cooperativity as defined in the free-standing systems, because in the range of concentrations where ethanol diminishes T_M , it has no effect on the cooperativity of the transition.¹⁸ Therefore, the transition widths we observe with QCM include sample geometry and lipid/surface coupling effects. At this point we can only speculate on the details. It is known that the two leaflets of the SLB melt at slightly different temperatures in SLBs prepared on smooth surfaces such as mica; this appears not to be the case on rough surfaces, such as silica.⁵¹ Here, lipid-surface interactions may contribute to the broadening of the transition, as may ethanol by preferentially partitioning into the outer leaflet. There is room for further studies here.

The final point concerns the value of the transition temperature that is detected by QCM. Our T_M values, taken at a mid-point between the heating and the cooling curves (Table I), are 24.9 ± 0.4 °C for the SLBs and 25.1 ± 0.4 °C for the SVLs. The value of the hysteresis that we observe, 1.4–1.7 °C, is typical of the scan rate we employed (0.2 °C/min).^{24,26,27} (For the dependence of the hysteresis on the temperature scan rates in SVLs, see Ref. 24; when extrapolated to zero scan rate, the hysteresis is similar to that observed at the low scan rates by DSC.⁵²) Wargenau and Tufenkji report a hysteresis of 3 °C, but at a scan rate of 0.4 °C/min.²⁵ Using their data for the cell temperature vs. scan rate (Table I in Ref. 25), we estimate that at a scan rate of 0.2 °C/min, the measured temperature is about 1 °C greater, than the actual temperature at the bilayer. Therefore, our T_M measurements are overestimated by ~ 1 °C. Taking this into account, our T_M values are very close indeed to the literature value of T_M for DMPC measured in free-standing systems (24 °C⁵). Ohlsson *et al.* also reported a transition temperature measured in the SVLs that was very similar to that of the free-standing lipids.²⁴ Losada-Pérez report a slightly higher T_M in the SVLs as compared to the free-standing lipids in one study²⁶ but a very close value in another.²⁶ However, Wargenau and Tufenkji²⁵ found a conspicuously low value of the transition temperature of DMPC SLBs (22.4–22.6 °C). They compared it with transition temperatures of DMPC SLBs supported on silica colloids measured by calorimetry, but neglected the very pronounced, and non-trivial, curvature effects that play a role in those systems.⁵³ Here we note in passing the excellent early work on the effect of curvature on the T_M in supported systems by Bayerl *et al.*,⁵⁴ and that a similar curvature-induced T_M depression occurs in the free-standing systems.⁵⁰ In other words, it is not clear whether the T_M for a solid-supported lipid bilayer should be lower than that for a free system (as Wargenau and Tufenkji appear to conclude), higher, or the same; it is also unclear that what factors it depend on (surface preparation, buffer composition, etc).

Further insight can, however, be gained from the T_M values for DMPC and DPPC in free-standing and solid-supported bilayer systems (not SVLs) tabulated by Mangiarotti and Wilke;⁵¹ the spread in the measured values is truly impressive, but most values are in fact higher in the supported bilayers. Their explanation for this is the loss of entropy due to the restriction of the out-of-plane lipid motion in supported systems. In some systems, this effect appears to suppress the

transition altogether.⁵⁵ In summary, the T_M values observed by the QCM are very close to the values for the free-standing systems—within a degree or, at the worst, two; this is much better than in the case of other techniques.⁵¹ Within this range, there remain some contradictions, but more precise determination must await further measurements.

An aspect that is missed in all of the discussions of T_M to date is the identity of the low-temperature phase. In the free-standing systems, the sequence of phases, from low temperature to high, is the gel phase ($L_{\beta'}$), the ripple phase ($P_{\beta'}$), and the fluid phase (L_{α}), but in single solid-supported bilayers ripple phase is absent: it is quenched by the interaction with the surface, presumably because of the significant amplitude of the ripples in the direction normal to the surface.^{20,56,57} Indeed, there have been no observations of the pre-transition ($L_{\beta'}-P_{\beta'}$) by QCM in the SLBs to date, including our work. We do not observe the pre-transition in the SVLs, either, but this may be due to the curvature effects described in Ref. 50 (in particular, see Figure 1 in that work), alone or in combination with the effect of the solid support.⁵⁴ The pretransition is seen in the multilayers which form over time when cycling the temperature in the presence of the lipid dispersion above the bilayer (Peschel *et al.*⁶¹).

CONCLUSIONS

We used a QCM to follow the main transition in supported DMPC systems of two different geometries (supported bilayers and supported vesicular layers). A model anesthetic (ethanol) could be detected via its effect on the parameters of the transition. Comparison of the results obtained with the two systems and the analysis of the frequency dependence allowed us to shed some light on the mechanism by which the QCM detects the transition: via the thickness changes and hydrodynamic effects in the supported vesicles, and via the thickness changes and viscoelastic effects in the supported bilayers. The values of the transition parameters, such as the transition temperature and width, reported by us and others, are critically discussed in light of our findings, suggesting fruitful avenues for further studies of these interesting systems.

SUPPLEMENTARY MATERIAL

See [supplementary material](#) for the temperature derivatives of the frequency.

ACKNOWLEDGMENTS

We much appreciate help with the construction of the cells by Andreas Böttcher. Dave Roberts wrote the software controlling the impedance analyzer. I.R. thanks the Biointerfaces in Technology and Medicine (BIF-TM) Program of the Helmholtz Association and the German Science Foundation (DFG Grant No. RE 2651/5-1) for funding and Professor Matthias Franzreb (IFG/KIT) for continuous support.

¹S. J. Singer and G. L. Nicolson, *Science* **175**, 720 (1972).

²K. Jacobson, E. D. Sheets, and R. Simson, *Science* **268**(5216), 1441 (1995).

³F. M. Menger, M. E. Chlebowski, A. L. Galloway, H. Lu, V. A. Seredyuk, J. L. Sorrells, and H. L. Zhang, *Langmuir* **21**(23), 10336 (2005).

- ⁴L. A. Bagatolli, J. H. Ipsen, A. C. Simonsen, and O. G. Mouritsen, *Prog. Lipid Res.* **49**(4), 378 (2010).
- ⁵A. Blume, *Thermochim. Acta* **193**, 299 (1991).
- ⁶S. L. Veatch and S. L. Keller, *Biochim. Biophys. Acta, Mol. Cell Res.* **1746**(3), 172 (2005).
- ⁷H. M. Seeger, M. L. Gudmundsson, and T. Heimburg, *J. Phys. Chem. B* **111**(49), 13858 (2007).
- ⁸T. Heimburg and A. D. Jackson, *Proc. Natl. Acad. Sci. U. S. A.* **102**(28), 9790 (2005).
- ⁹A. L. Hodgkin and A. F. Huxley, *Proc. R. Soc. B* **140**(899), 177 (1952).
- ¹⁰A. K. Lugli, C. S. Yost, and C. H. Kindler, *Eur. J. Anaesthesiol.* **26**(10), 807 (2009).
- ¹¹R. S. Cantor, *Biochemistry* **36**(9), 2339 (1997).
- ¹²R. J. Carlton, J. T. Hunter, D. S. Miller, R. Abbasi, P. C. Mushenheim, L. N. Tan, and N. L. Abbott, *Liq. Cryst. Rev.* **1**(1), 29 (2013).
- ¹³R. N. McElhaney, *Chem. Phys. Lipids* **30**(2-3), 229 (1982).
- ¹⁴M. A. Singer and L. Finegold, *Biophys. J.* **57**(1), 153 (1990).
- ¹⁵S. Mabrey, P. L. Mateo, and J. M. Sturtevant, *Biochemistry* **17**(12), 2464 (1978).
- ¹⁶T. J. McIntosh, H. Lin, S. Li, and C. Huang, *Biochim. Biophys. Acta* **1510** (1-2), 219 (2001).
- ¹⁷S. A. Simon and T. J. McIntosh, *Biochim. Biophys. Acta* **773**(1), 169 (1984).
- ¹⁸E. S. Rowe, *Biochemistry* **22**(14), 3299 (1983).
- ¹⁹S. M. Ohline, M. L. Campbell, M. T. Turnbull, and S. J. Kohler, *J. Chem. Educ.* **78**(9), 1251 (2001).
- ²⁰A. V. Hughes, S. A. Holt, E. Daulton, A. Soliakov, T. R. Charlton, S. J. Roser, and J. H. Lakey, *J. R. Soc. Interface* **11**(98), 20140447 (2014).
- ²¹H. P. Wacklin, *Curr. Opin. Colloid Interface Sci.* **15**(6), 445 (2010).
- ²²I. Reviakine, D. Johannsmann, and R. P. Richter, *Anal. Chem.* **83**(23), 8838 (2011).
- ²³C. A. Keller and B. Kasemo, *Biophys. J.* **75**(3), 1397 (1998).
- ²⁴G. Ohlsson, A. Tigerstrom, F. Hook, and B. Kasemo, *Soft Matter* **7**(22), 10749 (2011).
- ²⁵A. Wargenau and N. Tufenkji, *Anal. Chem.* **86**(16), 8017 (2014).
- ²⁶P. Losada-Pérez, K. L. Jiménez-Monroy, B. van Grinsven, J. Leys, S. D. Janssens, M. Peeters, C. Glorieux, J. Thoen, K. Haenen, W. De Ceuninck, and P. Wagner, *Phys. Status Solidi A* **211**(6), 1377 (2014).
- ²⁷P. Losada-Perez, M. Khorshid, D. Yongabi, and P. Wagner, *J. Phys. Chem. B* **119**(15), 4985 (2015).
- ²⁸I. Reviakine and A. Brisson, *Langmuir* **16**(4), 1806 (2000).
- ²⁹E. Tellechea, D. Johannsmann, N. F. Steinmetz, R. P. Richter, and I. Reviakine, *Langmuir* **25**(9), 5177 (2009).
- ³⁰R. C. Macdonald, R. I. Macdonald, B. P. M. Menco, K. Takeshita, N. K. Subbarao, and L. R. Hu, *Biochim. Biophys. Acta* **1061**(2), 297 (1991).
- ³¹R. Beck, U. Pittermann, and K. G. Weil, *Ber. Bunsengesellschaft Phys. Chem.* **92**(11), 1363 (1988).
- ³²D. Johannsmann, *The Quartz Crystal Microbalance in Soft Matter Research: Fundamentals and Modeling*, Soft and Biological Matter (Springer International Publishing, Switzerland, Heidelberg, 2015).
- ³³M. Rodahl, F. Hook, and B. Kasemo, *Anal. Chem.* **68**(13), 2219 (1996).
- ³⁴T. K. Lind, M. Cárdenas, and H. P. Wacklin, *Langmuir* **30**(25), 7259 (2014).
- ³⁵B. Seantier, C. Breffa, O. Felix, and G. Decher, *J. Phys. Chem. B* **109**(46), 21755 (2005).
- ³⁶D. Johannsmann, *Macromol. Chem. Phys.* **200**(3), 501 (1999).
- ³⁷D. Johannsmann, *Phys. Chem. Chem. Phys.* **10**, 4516 (2008).
- ³⁸K. K. Kanazawa and J. G. Gordon, *Anal. Chem.* **57**(8), 1770 (1985).
- ³⁹A. P. Borovikov, *Instrum. Exp. Tech.* **19**(1), 223 (1976).
- ⁴⁰I. Y. Hasan and A. Mechler, *Soft Matter* **11**(27), 5571 (2015).
- ⁴¹P. Losada-Pérez, M. Khorshid, and F. U. Renner, *PLoS ONE* **11**(9), e0163518 (2016).
- ⁴²N. Kucerka, Y. F. Liu, N. J. Chu, H. I. Petrache, S. T. Tristram-Nagle, and J. F. Nagle, *Biophys. J.* **88**(4), 2626 (2005).
- ⁴³J. F. Nagle and S. Tristram-Nagle, *Biochim. Biophys. Acta* **1469**(3), 159 (2000).
- ⁴⁴S. Tristram-Nagle, Y. Liu, J. Legleiter, and J. F. Nagle, *Biophys. J.* **83**, 3324 (2002).
- ⁴⁵C. H. Lee, W. C. Lin, and J. P. Wang, *Phys. Rev. E* **64**(2), 020901 (2001).
- ⁴⁶W. Rawicz, K. C. Olbrich, T. McIntosh, D. Needham, and E. Evans, *Biophys. J.* **79**(1), 328 (2000).
- ⁴⁷I. Reviakine, M. Gallego, D. Johannsmann, and E. Tellechea, *J. Chem. Phys.* **136**(8), 084702 (2012).
- ⁴⁸D. Johannsmann, I. Reviakine, and R. P. Richter, *Anal. Chem.* **81**(19), 8167 (2009).
- ⁴⁹G. Sauerbrey, *Z. Phys.* **155**(2), 206 (1959).
- ⁵⁰D. Marsh, A. Watts, and P. F. Knowles, *Biochim. Biophys. Acta, Biomembr.* **465**(3), 500 (1977).
- ⁵¹A. Mangiarotti and N. Wilke, *J. Phys. Chem. B* **119**(28), 8718 (2015).
- ⁵²R. Lewis, N. Mak, and R. N. McElhaney, *Biochemistry* **26**(19), 6118 (1987).
- ⁵³S. Ahmed and S. L. Wunder, *Langmuir* **25**(6), 3682 (2009).
- ⁵⁴T. Brumm, K. Jørgensen, O. G. Mouritsen, and T. M. Bayerl, *Biophys. J.* **70**(3), 1373 (1996).
- ⁵⁵B. L. Stottrup, S. L. Veatch, and S. L. Keller, *Biophys. J.* **86**(5), 2942 (2004).
- ⁵⁶C. Naumann, T. Brumm, and T. M. Bayerl, *Biophys. J.* **63**(5), 1314 (1992).
- ⁵⁷T. Kaasgaard, C. Leidy, J. H. Crowe, O. G. Mouritsen, and K. Jørgensen, *Biophys. J.* **85**(1), 350 (2003).
- ⁵⁸S. Mornet, O. Lambert, E. Dugué, and A. Brisson, *Nano Lett.* **5**(2), 281 (2005).
- ⁵⁹U. Seifert and R. Lipowsky, *Phys. Rev. A* **42**(8), 4768 (1990).
- ⁶⁰D. Johannsmann, I. Reviakine, E. Rojas, and M. Gallego, *Anal. Chem.* **80**(23), 8891 (2008).
- ⁶¹A. Peschel *et al.* (unpublished).